Geosciences and Engineering, Vol. 10, No. 15 (2022), pp. 154–172.
https://doi.org/10.33030/geosciences.2022.15.154

CHARACTERIZATION OF SOIL MOISTURE REGIME IN THE KAIROUAN REGION, TUNISIA

MOHAMED RAJHI[1], ENDRE DOBOS[2]
[1]*m.rajhi.inat@gmail.com, https://orcid.gov/0009-0006-2842-6240*
[2]*ecodobos@uni-miskolc.hu, https://orcid.org/0000-0002-9798-6376*

Abstract: Soil moisture (SM) is a major factor in agricultural practices and earth surface processes. Remote sensing has been widely applied to estimate the soil moisture. However, it is still a challenge to describe the horizontal and vertical availability and the redistribution of soil moisture in time. Therefore, it is necessary to develop a soil hydrological model capable of estimating soil moisture variation with high accuracy, which is important in planning and efficient use of land resources. Many methods based on optical or radar satellite data have already been developed to estimate SM under various climatic conditions and geographical distribution.

In this study, the agricultural region of Kairouan in central Tunisia was chosen as a study area. To perform SM estimation, we analyzed the relation between the optical satellite data indices, such as the NDVI and the NDWI, and the radar data. In addition, we studied the correlation between the different backscatters (V, H), optical data, DEM and the environmental covariates in order to extract the highest correlation and the most informative data sources. These results will be the input of our model. The combination of remote sensing data, the environmental variables and the associate geospatial data can provide valuable information for soil moisture estimation; this has the potential to support decision making to optimize the land use structure and the water resources management, and for use in precision agricultural applications.

Keywords: *Soil moisture, digital soil mapping, Remote sensing, Radar, Optical, Kairouan plain*

1. INTRODUCTION

Today, the world faces many challenges, such as food security, scarcity of water resources, climate change, and degradation and contamination of soils by salts, the so-called soil salinization. The social-economic reality of farmers in the center of Tunisia is very critical, because agriculture is the only means of making a living, but soil degradation and the uncontrollable variation in soil moisture threatens the lives of the inhabitants of these regions and the disruption of the demographic, economic and environmental ecosystem.

Soil moisture is described as the water available in the unsaturated soil surface derived from rainfall, snowmelt, or capillary attraction from groundwater [1]. The intricate connection between rainfall and soil moisture is of utmost importance in the field of land surface hydrology [2]. Therefore, there is a crucial need for an in-depth

study of the soil's characteristics and spatiotemporal distribution of the soil moisture in order to set up a monitoring system to aid in decision-making.

2. STUDY AREA

The governorate of Kairouan, located in the central region of the country *(Figure 1)*, occupies a strategic position at the regional and the national level. It extends over 658,000 ha and is in the form of a wide corridor of plains, which are limited to the west by mountainous areas and to the east by depressions made up of sebkhas. This natural environment is a made up of quite contrasting physical units (plains, hills, and mountains) offering climatic nuances and different resources, which necessarily generate specific uses and modes of occupation [3].

The study area, corresponding to the Merguellil basin, is included in the Kairouan plain. It is one of the three largest river basins on the southern flank of the Tunisian ridge, flowing into the Kairouan plain [4]. It is a relatively large homogeneous valley, but is also very sensitive to erosion [5]. The basin consists of two geographically dissimilar parts. The upstream section, which corresponds to the El Haouareb Dam's watershed, is mountainous. The Kairouan alluvial plain encompasses the downstream part [6].

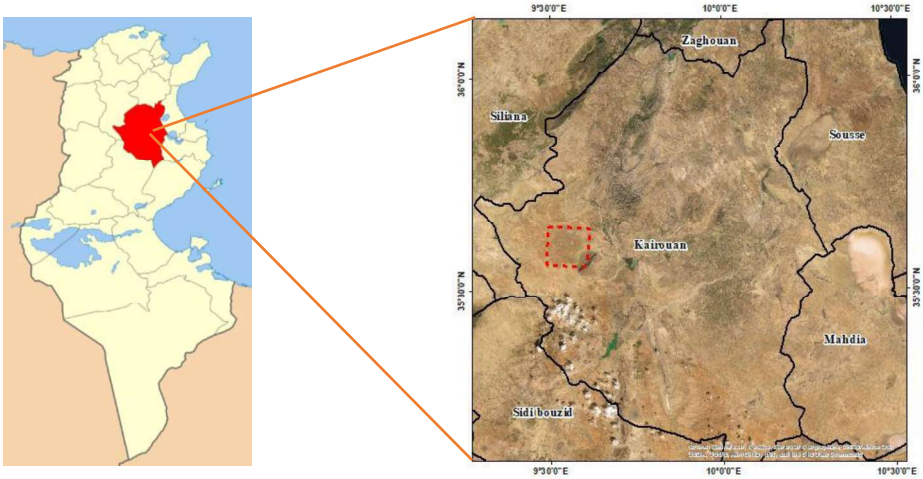

Figure 1
Study area – Merguellil downstream basin of the Kairouan plain [7]

The Merguellil upstream catchment (1200 km²) has a hilly topography (altitudes ranging from 200 to 1200 m, with a median elevation of 500 m) and diverse geology, morphology, vegetation, and land-use conditions. The Merguellil downstream watershed is part of the very large and flat Kairouan alluvial plain, which extends over about 3000 km² and with the altitude decreasing very gradually from 200 m to 80 m. [8] Our study area, the downstream part of the watershed, covered an area of 87 km² close to the dam, west of Kairouan city.

2.1. Geology

The upstream basin of Merguellil is composed of limestone, calcareous marl and marly sedimentary formations of the Cretaceous and Eocene *(Figure 2)*. The oldest formation dates from the Triassic. Our study area, the Merguellil downstream basin of the Kairouan plain, corresponds to a collapsed basin, where the Plio-Quaternary continental detrital filling can exceed 700 m in thickness. A small Cretaceous limestone structure outcrops at the western part of the basin located in the El Haouareb mountain [9].

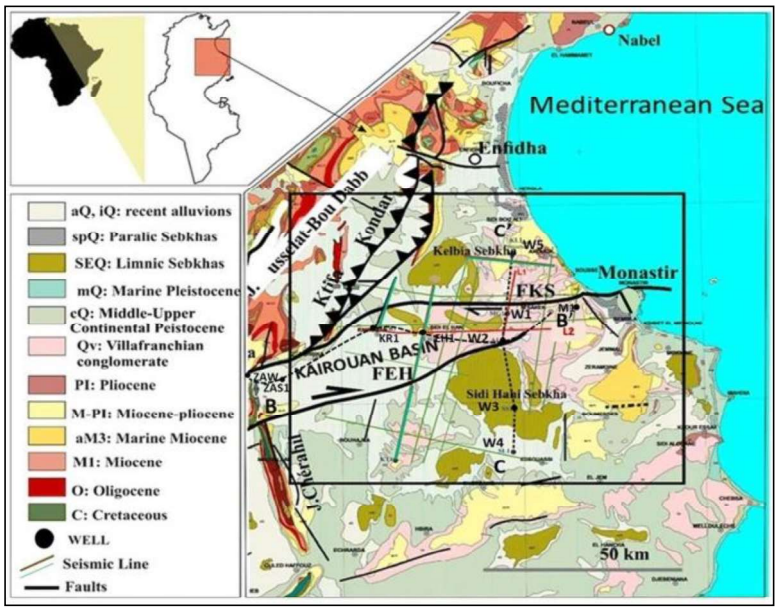

Figure 2
The geological map of the Kairouan Basin based on the 1/50,000 geologic map of Ben Hadj Ali et al. (1985) and the tectonic map of Khomsi et al. (2004) [10]

2.2. Climate of the Kairouan Region

The climate of central Tunisia, particularly in the Kairouan region, is distinguished by significant year-to-year and intra-year variations in rainfall. This fluctuation, along with water scarcity and drought periods, has a nagative impact on rain-fed agricultural productivity, resulting in unpredictable yields [11].

The study of several parameters, namely precipitation and temperature, serve to characterize the climate of the study area and to assess its degree of aridity. Indeed, these parameters have a significant impact on water availability [3].

The amount of precipitation varies a lot from year to year. The annual precipitation rate is less than 402 mm, with significant temporal and spatial variability. The daily mean temperature ranges from 9 °C in the winter to 34 °C in

the summer, with the hottest months being July and August *(Figure 3)*. The annual potential evapotranspiration rate is estimated to be around 1460 mm. [12]

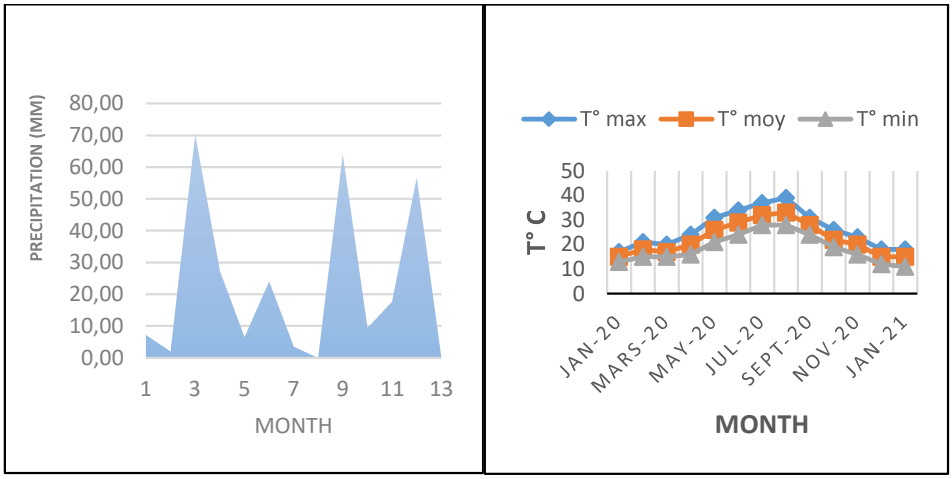

Monthly rainfall - Sidi Saad Station [13]

Monthly minimum, average and maximum temperature curve in Kairouan [14]

Figure 3
Precipitation and temperature in the study area [13–14]

3. MATERIALS AND METHODS

3.1. Materials

3.1.1. Sentinel 1 Imagery

SENTINEL-1 is an imaging radar mission providing continuous all weather, day-and-night imagery at C-band *(Table 1)*. The Sentinel-1 mission offers a range of distinct imaging modes, each with its own resolution, ranging from as low as 5 meters, and coverage extending up to 400 kilometers. It encompasses double polarization capability, rapid revisit times, and expedited product delivery. Additionally, precise spacecraft position and attitude measurements accompany every observation [15]. Sentinel-1B satellite imagery was used to characterize soil moisture in this study. The Sentinel-1B data used in the study has the following specifications:

Table 1
Specifications of the Sentinel-1B data used in the study [16]

Specifications	**Sentinel-1B**
Polarization	VV-VH
Imaging frequency	C-Band (5.4 GHz)
Resolution mode	5 meters
Acquisition times	January 2018–June 2020

3.1.2. Sentinel 2 Imagery

SENTINEL-2 is a European multi-spectral imaging mission with a wide and a high-resolution swath. The twin satellites, which are in the same orbit but phased at 180°, are designed to have a high revisit frequency of 5 days at the Equator. SENTINEL-2 is equipped with an optical payload that samples 13 spectral bands: four at 10 m, six at 20 m, and three at 60 m spatial resolution. The orbital swath is 290 kilometers wide [17].

During this research, the Sentinel 2 image will be used to calculate the values of the Normalized Difference Vegetation Index (NDVI) and Normalized Difference Water Index (NDWI).

3.1.3. Digital elevation data

Digital Elevation Models (DEMs) are used in geographic information systems to create relief maps by mapping terrain elevation. Since 2019, the Copernicus program has had a global and consistent high-resolution DEM available to all of its users for a wide range of applications. DEMs are classified into two types: digital surface models (DSM) and digital terrain models (DTM). DSM represents the Earth's surface envelope, including vegetation and man-made things like buildings and other forms of infrastructure, whereas DTM represents ground elevation. [18].

The Copernicus DEM is a Digital Surface Model (DSM) that depicts the Earth's surface, including structures, infrastructure, and vegetation. GLO-30 Public and GLO-90 are two Copernicus DEM instances provided by ESA *(Figure 4)*. At 90 meters, GLO-90 provides global coverage.

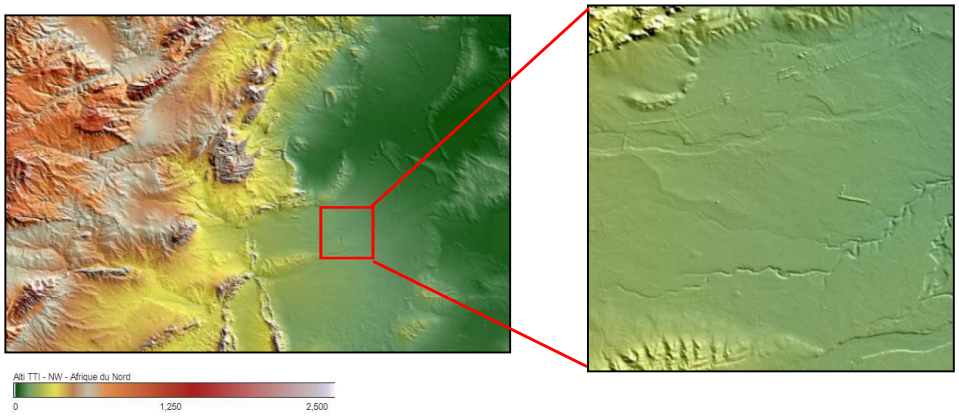

Figure 4
The DEM of the study area using Copernicus DEM GLO-30 m

The elevation shows that our study area is at the limit of the mountain's range, it is mainly consolidated materials, colluvial and alluvial materials coming from the mountain. This is what fills up our study area.

The geography of this study site is primarily defined by geology, with the plain dominating and the presence of mountains such as Jebel Trozza from the north-south direction. Clayey and clayey-sandy textures may be observed in the agricultural areas. As a result, topography is the main factor affecting soil formation in the study area.

3.2. Methods

My research strategy consists of collecting data from three sources: radar-sentinel 1, optical-sentinel 2, and Eras5-Global Precipitation Measurement (GPM). The first source will provide information about the Backscatter coefficient, while the second will provide information about the NDVI and NDWI, and the third will provide information about environmental factors such as temperature and rainfall. The obtained information will be processed at the advanced level in order to get the trained model, which will be calibrated using in-situ data. Furthermore, the model will enter the cycle of three phases, which are development, validation (with the support of in-situ data), and optimization, as seen in *Figure 5.*

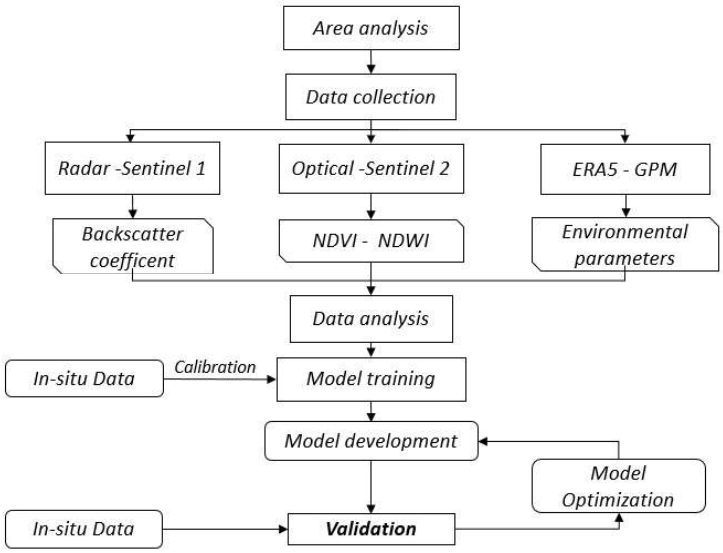

Figure 5
Methodological diagram of the model development

3.2.1. Data collection

The environmental covariates, Sentinel-1 (Backscatter coefficient), Sentinel-2 (NDVI and NDWI) and Digital terrain data were chosen as target explanatory variables to integrate. NDI is calculated as the difference between reflectance values in two bands divided by the sum of those values [19].

3.2.2. Extraction of Covariates

A combination of literature and statistical processing was used to select certain factors. According to the literature, covariates had to follow three criteria: first, they had to represent soil-forming elements; second, they had to have a direct link with SM; and third, they had to be readily available [20].

On the basis of these specifications, three kinds of data were chosen as environmental covariates: Sentinel-1 C-band, terrain data derived from DEM, and Sentinel-2 data to explain the biomass/vegetation influence on the SM [21].

3.2.3. Statistical Methods

In this paper, the statistical method used to describe and analyze soil moisture is the linear correlation. In a data-poor environment, linear regression produces more realistic spatial patterns over the landscape [22].

3.2.4. Characterization of Soil Moisture

Many researchers have developed models to characterize the soil moisture, and these models showed that soil moisture and backscattering coefficient have a fundamental relationship, e.g. [22]. The backscatter coefficient and Sentinel-2 data are considered main parameters that can help to characterize the soil moisture.

4. RESULTS AND DISCUSSION

4.1. Radar remote sensing

An optical image and a Sentinel-1 radar image are shown in *Figure 6* to visually analyze the area. The radar image (polarizations) is colored with an RGB composite: red = VH, green = VV, and blue = NDI, where NDI refers to the Normalized Difference Index of the VH and VV polarizations.

We can immediately distinguish the dominance of the bluish color, the greenish color and the presence of a reddish color at the level of the study area's south.

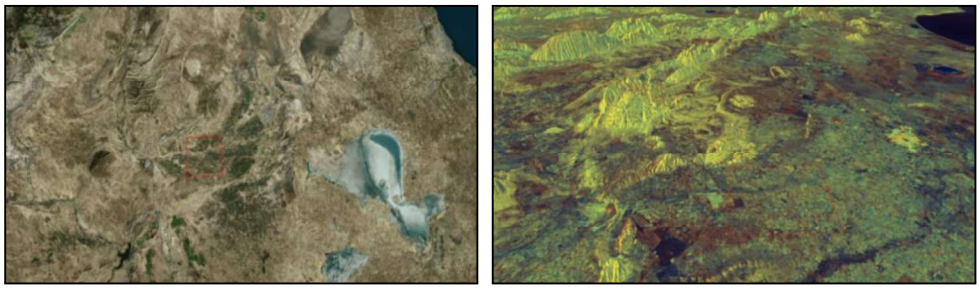

Figure 6
Optical image from the Bing Map and Sentinel-1B imagery of the study area

First of all, we did the visualization exercise with the RGB composite. A more detailed analysis on different polarizations *(Figure 7)* was made as follows:

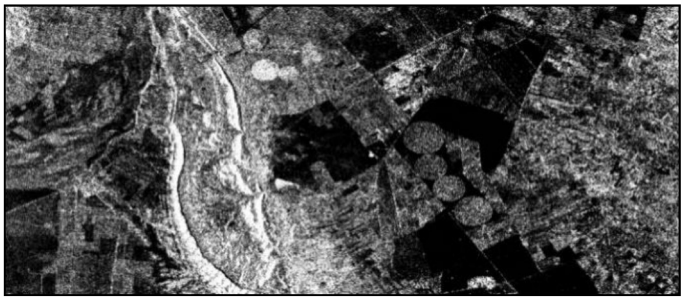

(a) Polarization VV

(b) Polarization VH

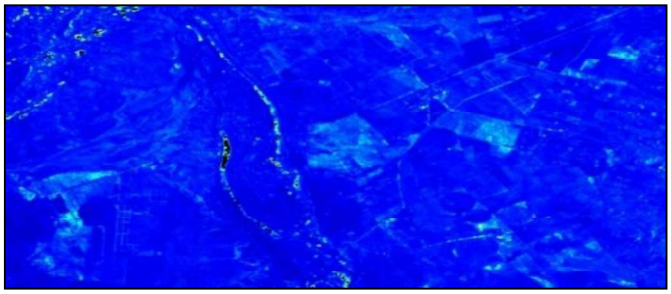

(c) Elevation

(d) Optical Image

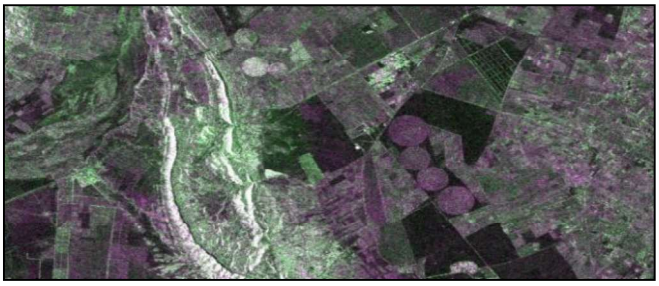

(e) RGB (VV, VH, VV)

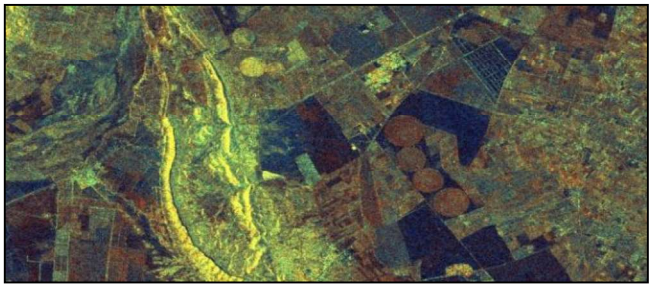

(f) RGB (VH, VV, NDI)

Figure 7

(a) *Polarization VV;* ***(b)*** *Polarization VH;* ***(c)*** *Elevation;* ***(d)*** *Optical Image;* ***(e)*** *RGB (VV, VH, VV);* ***(f)*** *RGB (VH, VV, NDI)*

Because SAR signals are prone to multiple scattering at various layers of vegetation, as well as at the subsurface or terrain level, interpreting vegetated parts of a SAR image demands the high level of understanding. The intensity of such scattering is heterogeneous in nature, varying from one SAR image to another, due to the changing nature of plant structures and closures.

The VH polarization produces comparable results to VV polarization, with the exception of greater separation of water masses and more precise information about the water region in the generated image [23]. The VV polarization is more informative for land use and for the vegetal cover analysis.

The wide histogram of the VV and the VH polarization image helps for a better discrimination of thematic classes including possible differentiation of identifying the open water, Irrigated area, soil roughness and the urban area. Although the RGB exercise of like-polarized and cross-polarized data can be considerably more informative.

Figure 7e and *7f* are a false-color composite of the Merguellil watershed's downstream. These images were acquired by the Sentinel-1 radar satellite. To aid the visual interpretation, the multiple channels of polarimetric data can be used to present the data in a colored image, in which certain image features are recognizable. As a simple example, a color image can be made using a VV = Red, VH = Green and VV = Blue channel assignment *(Figure 7e)*. This tends to "look realistic", as soil

water content reflections have a higher VH component than VV, and vegetation has a higher average than VH backscatter.

We use the Sentinel-1 SAR image in VV and HV polarization modes *(Figure 7f)* by presenting the VH/VV/NDI in RGB mode. Changes in the intensity of each color are related to surface conditions and covers; such as variations in surface roughness, biomasses, plant density, soil wetness, and soil types. Higher radar reflectance represented in VH/VV (yellow) is found in semi-consolidated and consolidated rocky material; lower backscatter in NDI polarization (dark blue) and VV/NDI (reddish) appears where erosional deposits and material related to fluvial erosion are abundant. Brighter colors are dominant where distinct bedrock layering can be observed. The units in bright yellow are typically caused by strong backscatter and VH polarization modes with VV represented as blue approaches zero.

The reddish areas in the image are the ploughed terrain. The yellow-greenish areas are cultivated areas with high soil moisture. The green areas are due to the relative high intensity of the VV channel, which is strongly correlated with the amount of biomass. The C-band VV and VH channels show the biomass variations over the entire region.

We can distinguish three major units in dark violet, brighter violet, and green colors using the Sentinel 1 SAR image in VV and HV polarization modes *(Figure 7e)* representing VH/VV/VV as RGB. Higher VV/VV (violet) radar reflectance is seen on plowed terrain with high roughness, but lower backscatter in VV polarization (dark violet) appears when uncultivated soils are abundant. We can distinct bedrock layering in the mountain by brighter colors predominant. Units in bright yellow are usually caused by high backscatter of VH polarization modes with VV, while the blue approaches zero. This can also indicate high soil moisture and a cultivated area.

4.2. Optical remote sensing

4.2.1. Characterization of the vegetation cover using NDVI

Figure 8 shows two images of the normalized difference vegetation index (NDVI) of the study area.

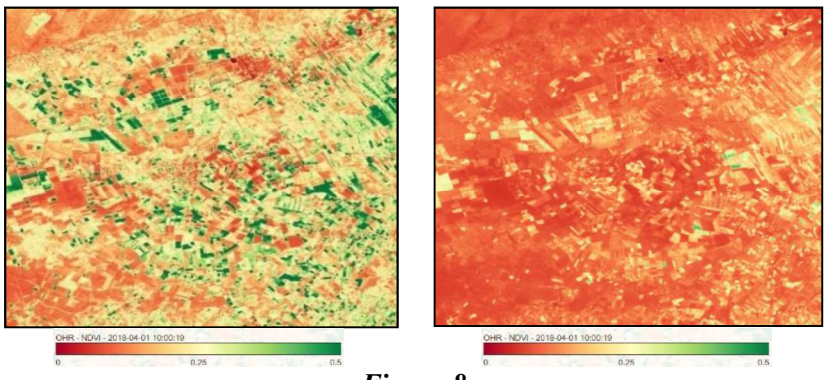

Figure 8

Normalized difference vegetation index (NDVI) of the study area

The image from January 2018 depicts wet conditions, while the one from July 2019 shows dry conditions. We can see a difference in vegetation cover between the two seasons; the first image displays a relatively dense vegetation cover, while the second image reveals sparse vegetation cover.

Figure 9a shows the variation of the normalized difference vegetation index (NDVI) of the study area. We can see the maximum and the minimum as well as the mean of the NDVI from January 2018 until December 2020. We see a big difference between the maximum and the maximum. This is explained by the difference between cultivated and non-cultivated areas, as well as plant life cycle differences. *Figure 9b* shows the variation of the NDVI between 2018 and 2020. We see the same trend of the three curves explained by the plant life cycles and the cultivation practices of farmers in the region.

$$\textbf{NDVI of the AOI} = \sum \textbf{Pixel value} / \textbf{N}$$

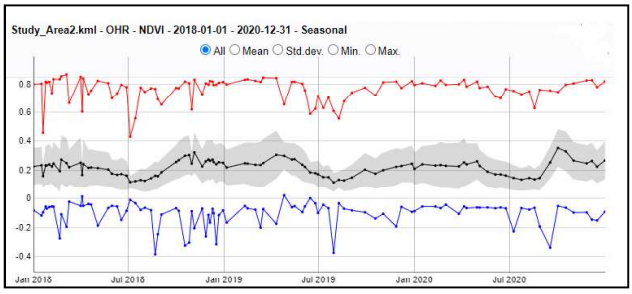

(a)

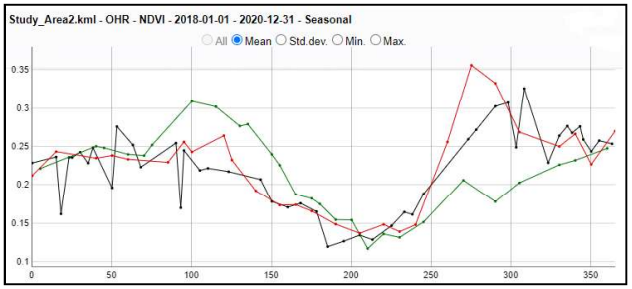

(b)

Figure 9

(a) *The maximum and the minimum of the NDVI value of the study area,*
(b) *variation of the NDVI value as a function of time*

4.2.2. Characterization of soil moisture using the water index

Figure 10 shows two images of the Normalized Difference Water Index (NDWI) of the study region. The image for June 2018 shows the dry time, but the image of October 2018 marks the beginning of the wet season. The first image shows various moist fields, which we can explain by the irrigated area, and the second image shows

land conditions following the rain, from which we can estimate that it had rained less than 48 hours before the date of the image.

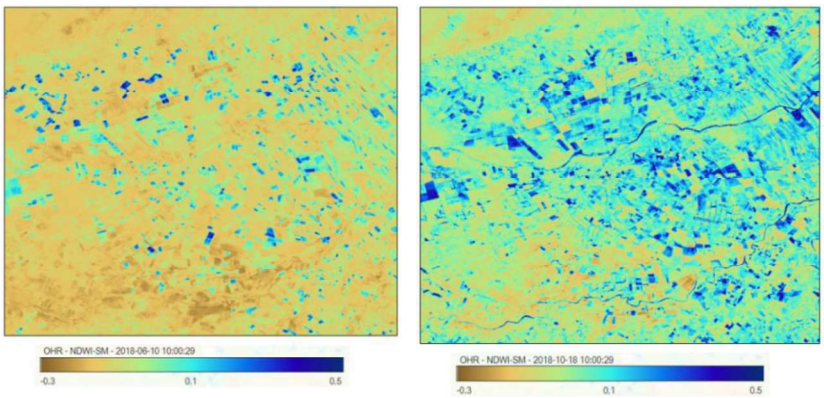

Figure 10

Normalized difference water index (NDWI) of the study area

The variation of the water index (NDWI) of the study area is depicted in *Figure 11a*, where we can observe the maximum, the minimum, and the mean of the NDWI from January 2018 to December 2020. In addition, we can notice a large gap between the maximum and the minimum, which demonstrates a large amount of land use, plant cover, and soil variability, indicating that soil moisture is determined more by land use and soil variability than by climate. *Figure 11b* shows the change in the NDWI from 2018 to 2020, and we can notice the similar pattern of the three curves described by the plant life cycles and the weather in the region.

The NDVI and NDWI results show that the study area is classified into several basic categories, which represent variations in land use/land cover and different crops. In our study area, conventional irrigation is dominant. The results show that vegetable crops such as tomatoes, peppers and plots of olive trees are the dominant crops in the study area.

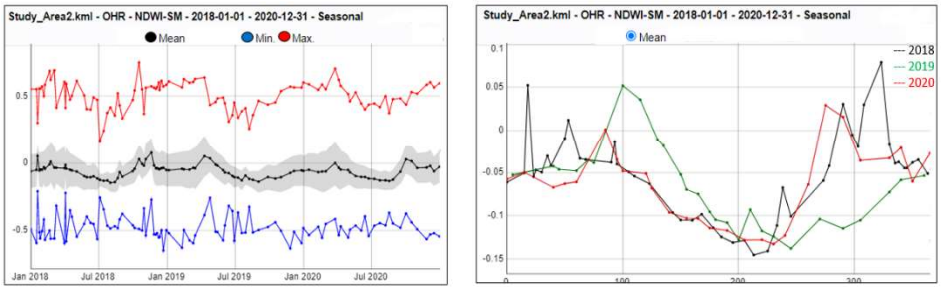

(a) (b)

Figure 11

(a) *The maximum and the minimum of the NDWI value of the study area,*
(b) *variation of the NDWI value as a function of time*

Pilot Area – Sub-pilot areas

To better understand the soil moisture regime and the impact of the environment parameters, we will focus our study on one parcel. On this parcel we will select two sub-pilot areas which are exposed to the same conditions and the same environment. We can visually observe the difference between the two sub-pilots; the plant cover of Pilot 1 seems less developed and less dense than Pilot 2.

A study was conducted on NDVI and NDWI on the two sub-pilots *(Figure 12)* for a period of three years between 2018 and 2020.

Figure 12
Normalized difference vegetation index (NDVI) of Pilots 1 and 2

During the rainy season, the NDVI of Pilot 1 is lower than that of Pilot 2 *(Figure 13)*, while it is higher during the dry seasons.

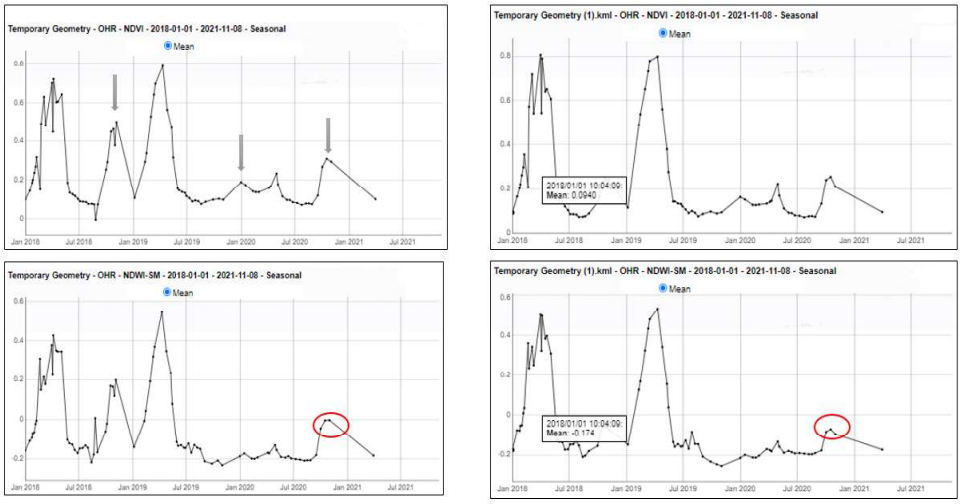

Pilot 1 Pilot 2

Figure 13
Comparison between the NDVI (top) and the NDWI (bottom)of sub-pilot areas

The NDWI of Pilot 1 is higher than that of Pilot 2 during both the dry and rainy seasons. Here, we can interpret that the type of soil in Pilot 1 and Pilot 2 is different, and that the soil of Pilot 1 has a higher water retention capacity than the soil of the pilot 2. We can also explain why the value of NDVI is lower for pilot 1 than pilot 2, despite a higher water retention capacity, by the soil of pilot 1 being close to reaching water saturation, which is not favorable to the development of vegetation.

4.2.3. Correlation between the NDVI and the NDWI

A statistical analysis was made between the NDVI and NDWI values of the study area between 2018 and 2020. *Figure 14* shows the results of the linear correlation between the two indices NDVI and NDWI. We see a strong correlation between the two parameters, with R = 0.79 and R^2 = 0.64.

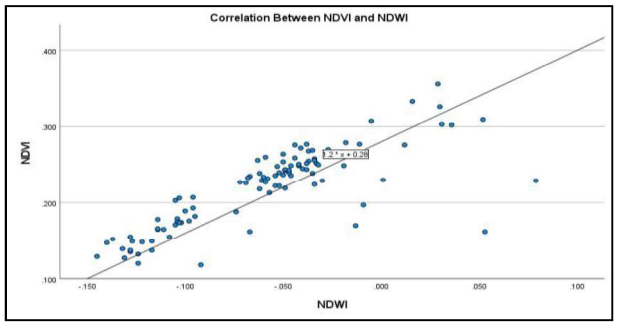

Figure 14
Correlation between NDVI and NDWI

This result is explained by the strong correlation between the water and the biomass in the nature and also technically the two parameters are based on the near-infrared as one of the major points.

We noticed some points a little away from the line of the correlation curve that raised questions, which is why we investigated further to check the reasons. As shown below, a measure of the correlation coefficient was performed between the means of NDWI-NDVI, the maximums of NDWI-NDVI and the minimums of NDWI-NDVI.

(a) Pilot 3 (b) Pilot 4 (c) Pilot 5

Figure 15
Delimitation of Pilot 3, Pilot 4 and Pilot 2

The results reveal that maximums and means have a higher correlation, whereas minimums have a lower correlation. Furthermore, a small pilot area (Figure 15a) is used for validation; its correlation coefficients are calculated as shown in the pilot curves below *(Figure 17)*, and this pilot reveals strong correlations between maximums, means, and minimums. The weak correlation between the minimums in the study area *(Figure 16)* can be explained by the presence of free water or by the presence of certain urban areas. In addition, the out-of-range points could be explained by a technical error while the output results are symbolic of the same date, this error could be considered as noise.

To be sure of this assumption, we worked on two other small pilots (4 and 5) who have the same occupation. Olive trees occupy Pilot 4, while Pilot 5 is covered by horticulture. The results show a strong correlation between the means of NDWI-NDVI and the maximum of NDWI-NDVI; on the other hand the minimum of NDWI-NDVI shows a correlation coefficient lower than the average and the maximum and is also unpredictable. We can explain the weak and unpredictable results of the minimum NDWI-NDVI by the presence of different land cover, which can be wet without vegetation, and we can say that the minimum is not representative.

Pilots 4 and 5 (*Figure 18* and *Figure 19*) shows the same out rang points as the first and the second analysis. That is why we can consider the out rang points as noise.

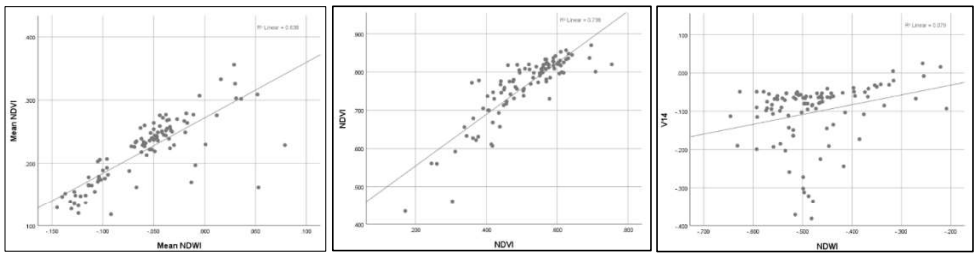

$R = 0.79$ $R^2 = 0.64$ $R = 0.859$ $R^2 = 0.638$ $R = 0.28$ $R^2 = 0.079$

Figure 16

Correlation between the NDWI and NDVI of the study area

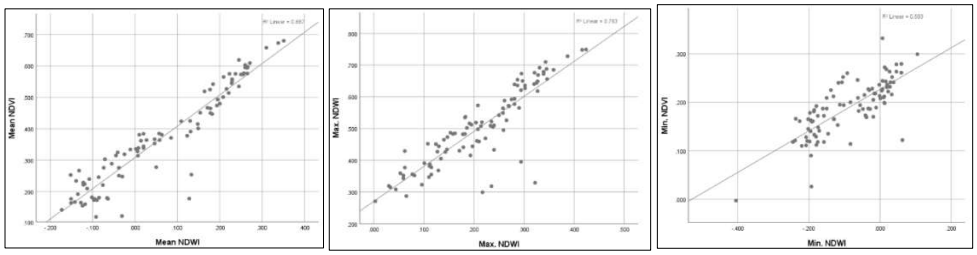

$R = 0.87$ $R^2 = 0.89$ $R = 0.94$ $R^2 = 0.76$ $R = 0.764$ $R^2 = 0.58$

Figure 17

Correlation between the NDWI and NDVI of Pilot 3

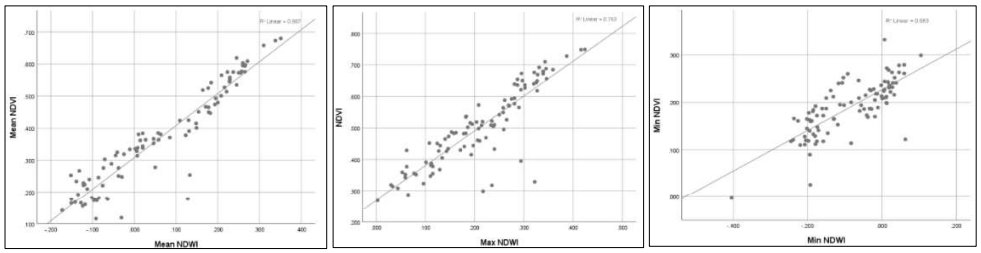

R = 0.94 R^2 = 0.89 R = 0.87 R^2 = 0.76 R = 0.76 R^2 = 0.58

Figure 18

Correlation between the NDWI and NDVI of Pilot 4

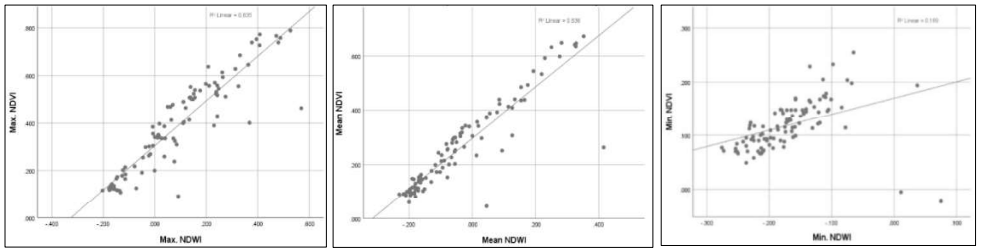

R = 0.91 R^2 = 0.84 R = 0.91 R^2 = 0.84 R = 0.41 R^2 = 0.17

Figure 19

Correlation between the NDWI and NDVI of Pilot 5

5. CONCLUSIONS

In this study, the correlation method was used to characterize the soil moisture regime using Sentinel-1B C-band SAR satellite data, the Normalized difference vegetation index (NDVI), and the Normalized difference water index (NDWI). Five pilots in the study area were chosen and analyzed to identify the relation between the optical and radar satellite data and the soil moisture. In order to extract the highest correlation and most informative data sources, we evaluated at the correlation between different backscatters (V, H), optical data, DEM, and environmental variables. The Normalized difference vegetation index (NDVI), the Normalized difference water index (NDWI), the Radar data (VV and VH polarization) and the soil types showed a strong correlation with the wetness and the vegetation conditions. The applied basic cognitive and statistical tools combined with local knowledge has demonstrated that these datasets have comparative potential in explaining the soil water regime and its relationship to the vegetation condition. The method is a promising and useful tool that may be used to characterize the soil moisture regime in the region. The environmental covariates should be statistically tested through the correlation methods to determine which covariates had the highest correlation with soil moisture.

REFERENCES

[1] Petropoulos, G. P., Griffiths, H. M., Dorigo, W., Xaver, A., Gruber, A. (2013). Surface Soil Moisture Estimation: Significance, Controls, and Conventional Measurement Techniques. In: Petropolous, G. (ed.). *Remote Sensing of Energy Fluxes and Soil Moisture Content*. CRC Press, Boca Raton, Louisiana, pp. 29–48.

[2] Sehler, R., Li, J., Reager, J. T., Ye, H. (2020). Investigating Relation-ship Between Soil Moisture and Precipitation Globally Using Remote Sensing Observations. *Journal of Contemporary Water Research & Education*. https://doi.org/10.1111/j.1936-704X.2019.03324.x

[3] Sarra Bel Haj Salem (2013). Utilisation des traceurs environnementaux pour l'étude des mode de recherche des eaux du bassin de Zéroud (Plaine de Kairouan). pp. 51, 2, pp. 272–284, doctoral dissertation, University ofSfax, Sfax, Tunisia..

[4] M, Zribi, A. C, and B. N. (2020). Editorial for the special issue Soil moisture retrieval using radar remote sensing sensors. *Remote Sens.*, Vol. 12, No. 7. https://doi.org/10.3390/rs12071100

[5] Le Goulven, Patrick & Leduc, Christian & Bachta, Mohammed & Poussin, Jean-Christophe. (2009). Sharing scarce resources in a Mediterranean River Basin: Wadi Merguellil in central Tunisia. International Water Management Institute Books, Reports H042452, International Water Management Institut.

[6] Taoufik Hermassi, Mohamed Amine Cherif, Hamadi Habaieb (2014). Solid Transport study at the Merguellil watershed, central Tunisia: case study of Ettiour and Rajela watersheds. *La Houille Blanche*, 100, 4, pp. 88–96. https://doi.org/10.1051/lhb/2014043

[7] Lacombe, G. (2007). Evolution and uses of water resources in a semi-arid managed watershed. The case of Merguellil in Central Tunisia. Doctoral dissertation at the Montpellier University, Science and Techniques of Languedoc.

[8] Chulli, B., Favreau, G., Jebnoun, N., Bédir, M. (2011). Impact of changing climate in the Kairouan Hydrological basin (central Tunisia). *Journal of Environmental Science and Engineering*, 5, pp. 682–688.

[9] Safouan Ben Ammar, Kamel, Zouari, Christian Leduc., Jemaiel, M'Barek. (2006). Isotopic characterization of the dam—aquifer water transfer in the Merguellil catchment (Kairouan Plain, central Tunisia). *Hydrological Sciences Journal*, 51, 2, pp. 272–284, https://doi.org/10.1623/hysj.51.2.272.

[10] Bédir, M., Soltani, A., Mohamed, A. B. et al. (2020). Cretaceous petroleum system modeling of Kairouan Basin in eastern Tunisia. *Arab. J. Geosci*., 13, 683, https://doi.org/10.1007/s12517-020-05550-0.

[11] Mougou, R., Mansour, M., Iglesias, A. et al. (2011). Climate change and agricultural vulnerability: a case study of rain-fed wheat in Kairouan, Central Tunisia. Reg Environ Change 11 (Suppl 1), pp. 137–142. https://doi.org/10.1007/s10113-010-0179-4

[12] Hamdi, Mohamed & Tarhouni, Jamila & Zagrarni, Mohamed & Laouini, Ghassen & Müller, Hans. (2017). Assessment of groundwater flow dynamic using GIS tools and 3D geological modeling: Case of Sisseb El Alem-Nadhour Saouaf basin, Northeastern Tunisia. 19. 2028-9324. *International Journal of Innovation and Applied Studies*, Vol. 19, No. 1, Jan. 2017, pp. 226–238, Innovative Space of Scientific Research Journals.

[13] Safouane Mouelhi , Saida Nemri , Sihem Jebari and Mohamed, Slimani (2016). Using the Markov Chain for the Generation of Monthly Rainfall Series in a Semi-Arid Zone. *Open Journal of Modern Hydrology*, 6, pp. 51–65. https://doi.org/10.4236/ojmh.2016.62006

[14] Fletcher, Karen (ed.) (2012). SENTINEL 1: ESA's Radar Observatory Mission for GMES Operational Services. European Space Agency. https://sentinel.esa.int/web/sentinel/user-guides/sentinel-1-sar/overview.

[15] Fletcher, Karen (ed.) (2012). SENTINEL 1: ESA's Radar Observatory Mission for GMES Operational Services. European Space Agency. https://sen tinels. copernicus.eu/web/sentinel/missions/sentinel-1/overview/mission-sum mary.

[16] Roland Meynart, Steven P. Neeck, Haruhisa Shimoda (2013). Sensors, Systems, and Next-Generation Satellites XVII. Proceedings of SPIE, Volume 8889, Article 88890K, https://doi.org/10.1117/12.2028755.

[17] Franks, Shannon, and Rajagopalan Rengarajan (2023). Evaluation of Copernicus DEM and Comparison to the DEM Used for Landsat Collection-2 Processing. *Remote Sensing*, 15, No. 10, p. 2509. https://doi.org/10.3390/rs15102509

[18] Chen, F., Van de Voorde, T., Roberts, D., Zhao, H., Chen, J. (2021). Detection of Ground Materials Using Normalized Difference Indices with a Threshold: Risk and Ways to Improve. *Remote Sens*., 13, p. 450. https://doi.org/10.3390/rs13030450

[19] Dobos, Endre, Daroussin, Joël, Montanarella, Luca (2010). A Quantitative Procedure for Building Physiographic Units Supporting a Global Soter Database. *Hungarian geographical bulletin*, 59, pp. 181–205.

[20] Dobos, E., Micheli, E., Baumgardner, M. F., Biehl, L., Helt, T. (2000). Use of combined digital elevation model and satellite radiometric data for regional soil mapping. *Geoderma*, Vol. 97, No. 3–4, pp. 367–391. https:doi.org/10.1016/S0016-7061(00)00046-X

[21] Kibirige, D., Dobos, E. (2020). Soil moisture estimation using citizen observatory data, microwave satellite imagery, and environmental covariates. *Water (Switzerland)*, Vol. 12, No. 8, https://doi.org/10.3390/W12082160.

[22] Qian Zhang, Xiangnan Liu, Meiling Liu, Xinyu Zou, Lihong Zhu and Xiaohao Ruan (2021). Comparative Analysis of Edge Information and Polarization on SAR-to-Optical Translation Based on Conditional Generative Adversarial Networks. *Remote Sens*., 13, p. 128, https://doi.org/10.3390/rs13010128.